

Electronic Supplementary Material (ESI) for Dalton Trans.

"Slow magnetic relaxation for cobalt(II) complexes in axial bipyramidal environment: an $S = \frac{1}{2}$ spin case."

Evangelos Pilichos,^a Mercè Font-Bardia,^b Joan Cano,^c Albert Escuer,^{*a} and Júlia Mayans ^{*a}

^a Departament de Química Inorgànica i Orgànica, Secció Inorgànica and Institute of Nanoscience (IN²UB) and Nanotecnology, Universitat de Barcelona, Martí i Franquès 1-11, Barcelona-08028, Spain.

^b Departament de Mineralogia, Cristal·lografia i Dipòsits Minerals, Universitat de Barcelona, Martí Franqués s/n, 08028 Barcelona (Spain) and Unitat de Difracció de R-X. Centre Científic i Tecnològic de la Universitat de Barcelona (CCiTUB), Solé i Sabaris 1-3. 08028 Barcelona.

^c Instituto de Ciencia Molecular (ICMol), Universitat de València, 46980 Paterna (València), Spain

1- Characterization.

Fig. S1. Powder X-ray spectra of the reference complex **1** and its diluted analogous **1D**.

Fig. S2. IR spectra for complexes **1** and **1D**

Fig. S3. IR spectra for complexes **2** and **3**.

2-Structural aspects.

Table S1. SHAPE measures for the Co^{II} cation of complex **1**.

Fig. S4. Plot of the coordination sphere of the Co^{II} cation for complex **1**,

Fig. S5. Detail of the H-bonds promoted for complex **1**.

Table S2. Bond parameters for the bifurcated H-bonds corresponding to complex **1**.

Fig. S6. Molecular structure of complex **2R** from the partial structure resolution.

3-Magnetic data.

Fig. S7. Left, magnetization vs. field for complexes **1**, **2R** and **3SS**. Right, reduced magnetization for complex **1**.

Fig. S8. χ_M'' dependence of the transverse field for complexes **1** and **2R**.

Fig. S9. $\chi_M'(T)$ and $\chi_M'(v)$ for complexes **1**, **1D** and **2R**.

Fig. S10. Argand plots for complexes **1**, **1D** and **2R**.

Fig. S11. Log-log plot for complex **1**.

Fig. S12. Plot of $\ln(1/2\pi v)$ vs. T^1 from the $\chi_M''(T)$ data for complexes **1**, **1D** and **2**.

Fig. S13. Plot of τ vs. inverse of temperature showing the low temperature increase of t for the diluted complex **1D**.

1- Characterization.

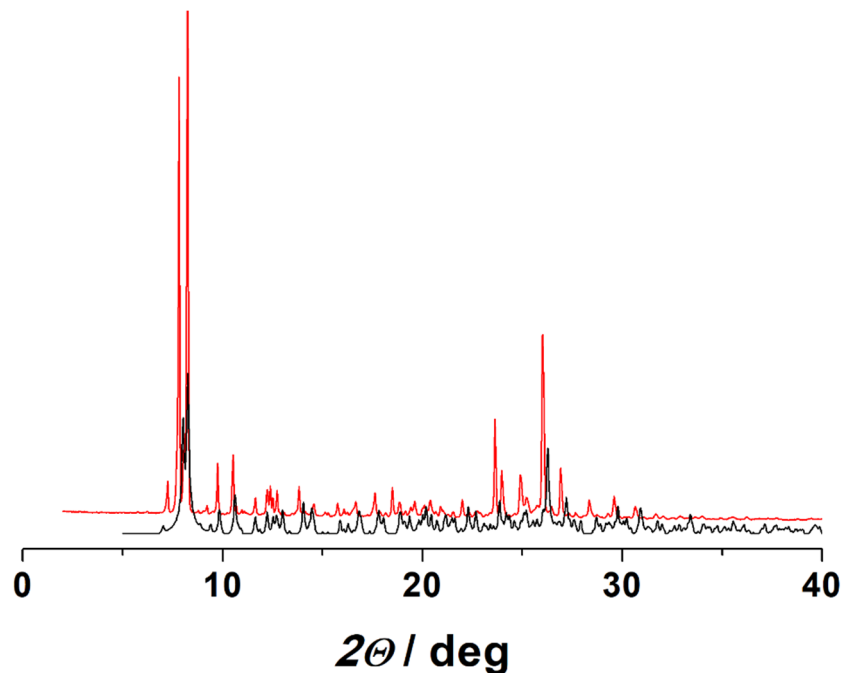


Fig. S1. Powder X-ray spectra of the reference complex **1** (black line) and its diluted analogous **1D**.

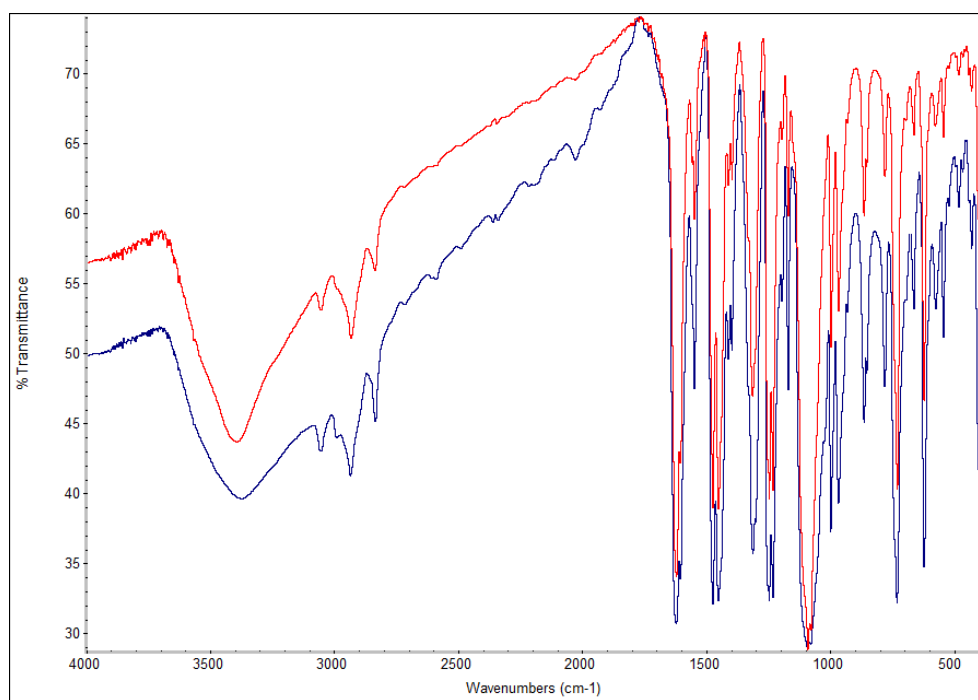


Fig. S2. IR spectra for complexes **1** (red) and **1D**. Characteristic bands: st. C-H 3000-2800 cm^{-1} ; N=C iminic $\sim 1600 \text{ cm}^{-1}$; st. ClO_4^- 1075 cm^{-1} ; $\delta \text{ ClO}_4^-$ 620 cm^{-1} .

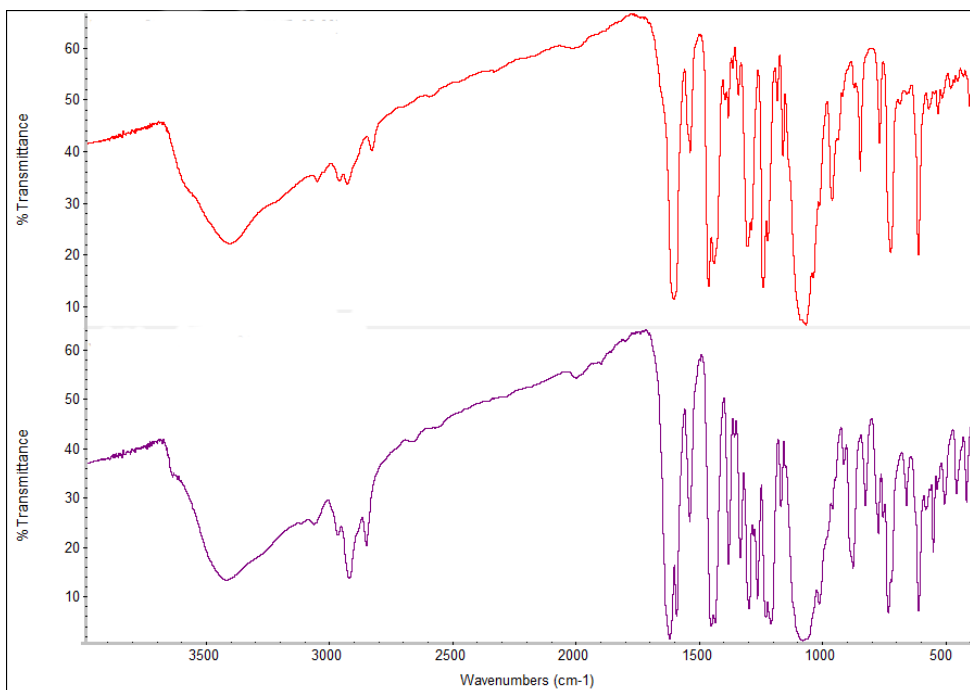


Fig. S3. IR spectra for complexes **2** (top) and **3** (bottom).

2-Structural aspects.

Table S1. SHAPE measures for the Co^{II} cation of complex **1**. $S(P) = 0$ corresponds to a structure fully coincident in shape with the reference polyhedron P, regardless of size and orientation. The closest polyhedron is highlighted in red.

$S(\text{vOC-5})$	6.80	$S(\text{PBPY-7})$	1.64
$S(\text{TBPY-5})$	6.82	$S(\text{COC-7})$	8.17
$S(\text{SPY-5})$	6.79	$S(\text{CTPR-7})$	6.59
$S(\text{JTBPY-5})$	8.81	$S(\text{JPBPY-7})$	3.60

Ideal ML₅ polyhedra: vOC-5 (C₄v) Vacant octahedron; TBPY-5 (D₃h) Trigonal bipyramidal; SPY-5 (C₄v) Spherical square pyramid; JTBPY-5 (D₃h) Johnson trigonal bipyramid J12.

Ideal ML₇ polyhedra: PBPY-7 (D₅h) Pentagonal bipyramid; COC-7 (C₃v) Capped octahedron; CTPR-7 (C₂v) Capped trigonal prism; JPBPY-7 (D₅h) Johnson pentagonal bipyramid J13; JETPY-7 (C₃v) Johnson elongated triangular pyramid J7.

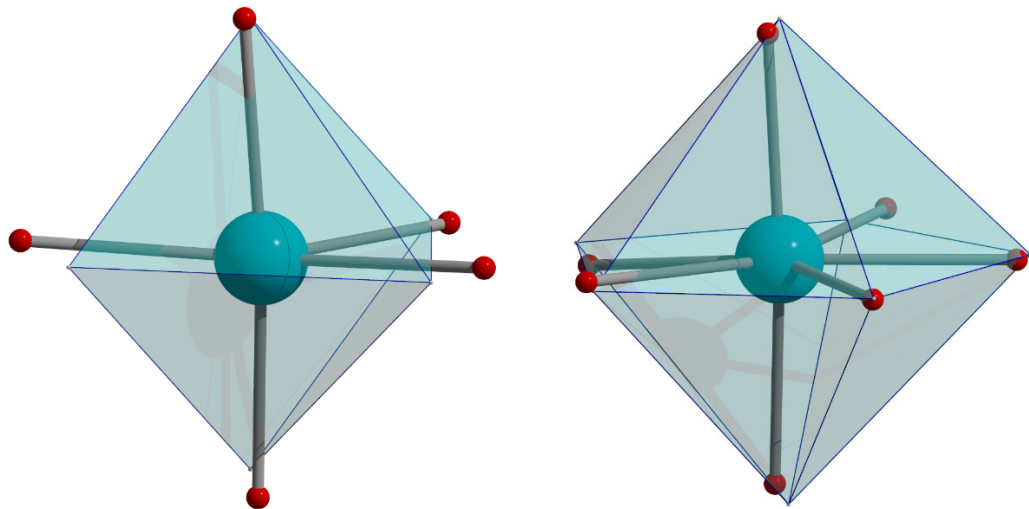


Fig. S4. Plot of the coordination sphere of the Co^{II} cation for complex **1**, referenced to the ideal polyhedra trigonal bipyramidal (left) and pentagonal bipyramidal (right).

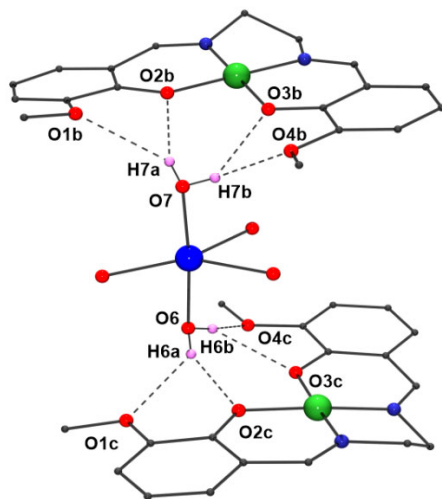


Fig. S5. Detail of the H-bonds promoted by the axially coordinated water molecules and the capping [NiL1] fragments for complex **1**.

Table S2. Bond parameters for the bifurcated H-bonds corresponding to complex **1**.

	$d \text{ O}\cdots\text{O}' (\text{\AA})$		$d \text{ H}\cdots\text{O}' (\text{\AA})$		$\text{O-H}\cdots\text{O} (\text{deg.})$
O6···O1c	2.976(4)	H6a-O1c	2.29(3)	O6-H6a···O3c	127(2)
O6···O2c	2.761(4)	H6a-O2c	2.10(2)	O6-H6a···O4c	159(3)
O6···O3c	2.848(4)	H6b-O3c	2.35(3)	O6-H6b···O1c	135(3)
O6···O4c	2.861(4)	H6b-O4c	2.03(2)	O6-H6b···O2c	152(3)
O7···O1b	3.010(4)	H7a-O1b	2.46(3)	O7-H7a···O1b	127(3)
O7···O2b	2.804(4)	H7a-O2b	2.04(3)	O7-H7a···O2b	160(3)
O7···O3b	2.860(4)	H7b-O3b	2.34(4)	O7-H7b···O3b	123(3)
O7···O4b	2.971(5)	H7b-O4b	2.20(4)	O7-H7b···O4b	161(3)

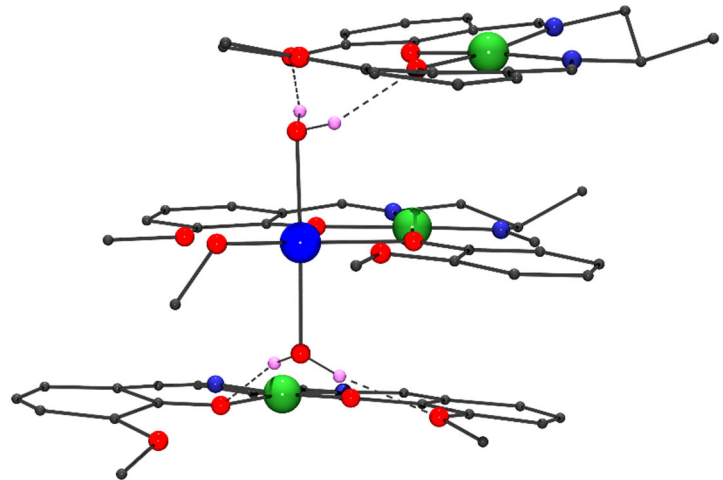


Fig. S6. Molecular structure of complex **2R** from the partial structure resolution.

3-Magnetic data.

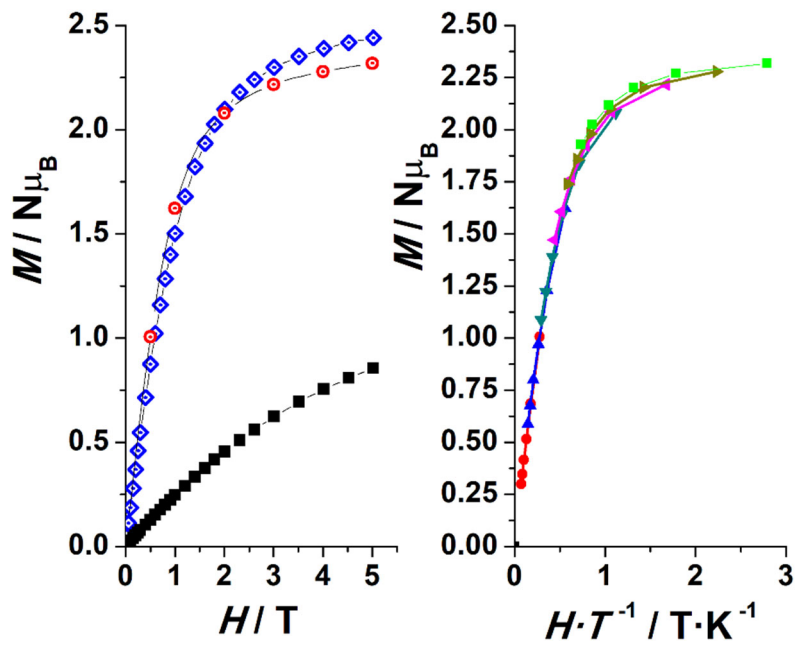


Fig. S7. Left, magnetization vs. field for complexes **1** (red circles), **2R** (blue diamonds) and **3SS** (black squares). Right, reduced magnetization for complex **1** showing the superimposable plots in the 1.8-6.8 range of temperature (increment 1 K).

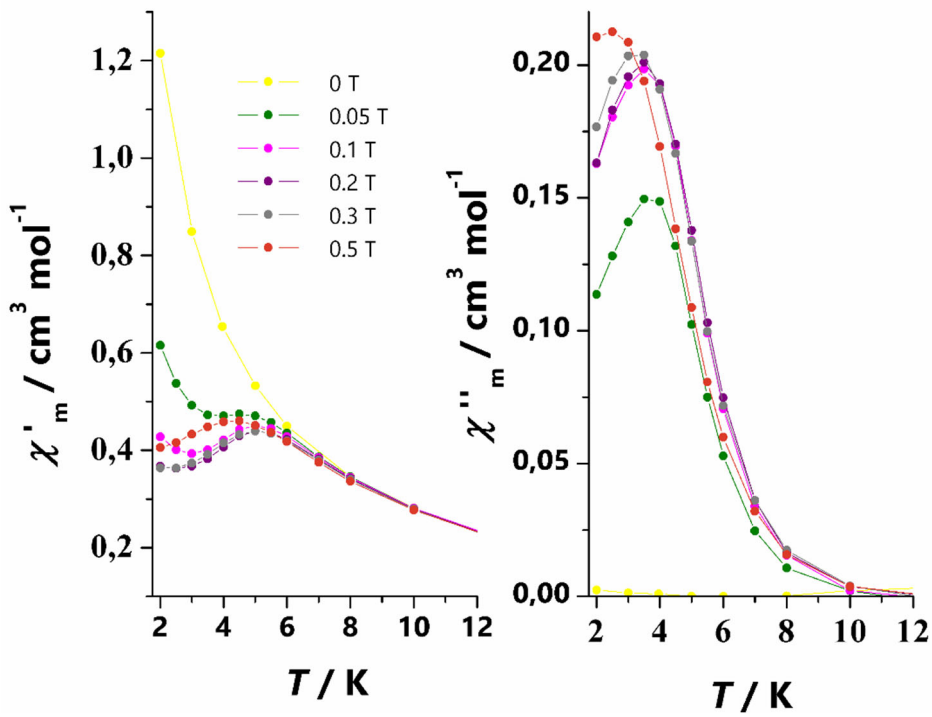
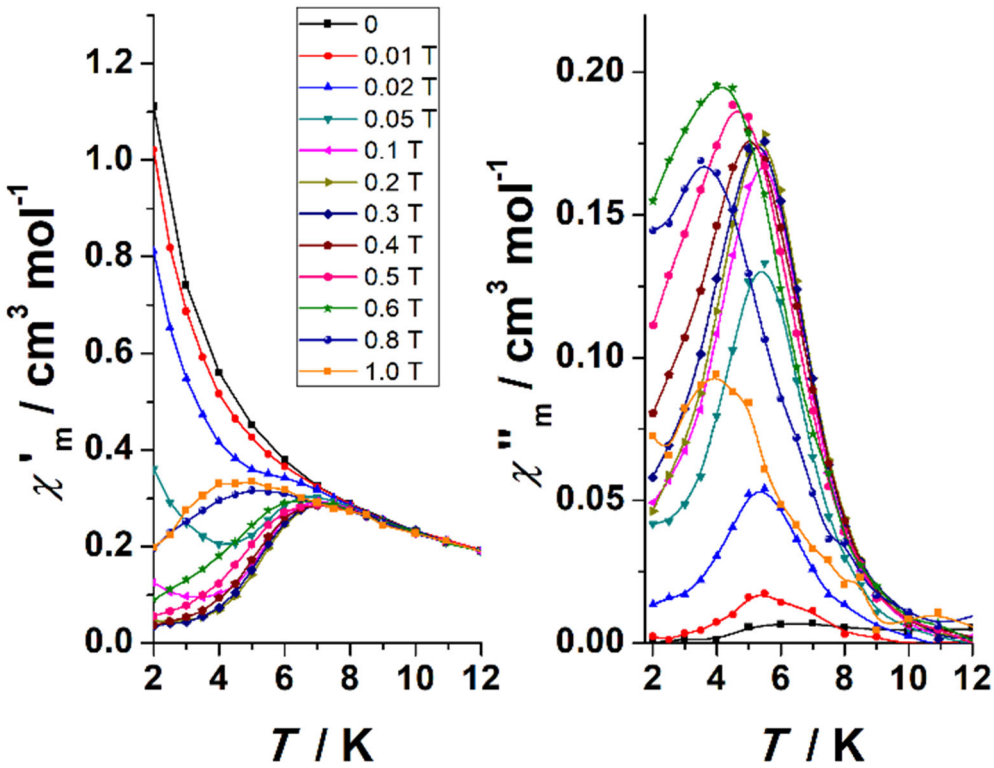


Fig. S8. χ_M'' dependence of the transverse field for complexes **1** (top) and **2R** (bottom).

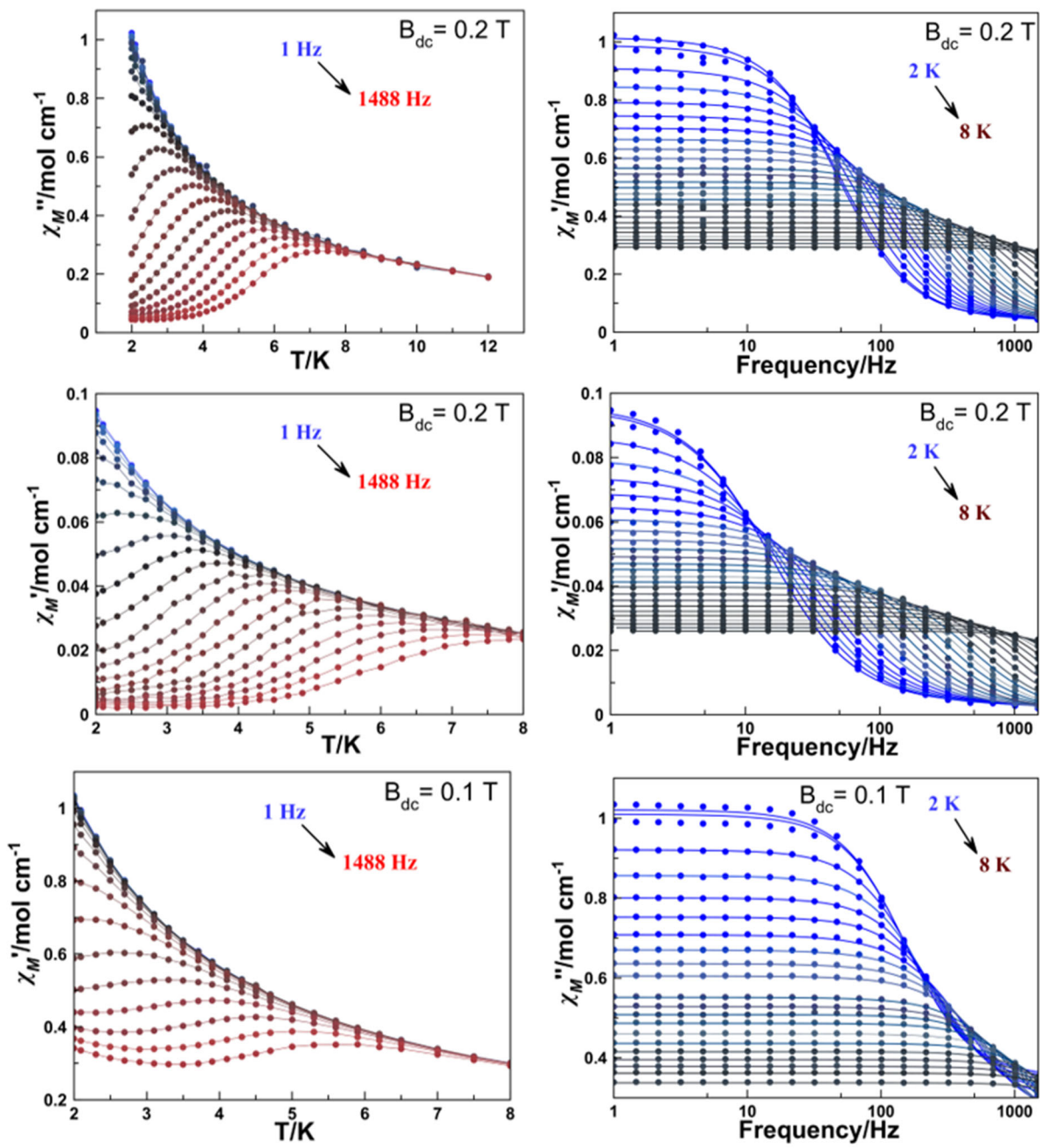


Fig. S9. $\chi_M'(T)$ and $\chi_M''(v)$ for complexes **1**, **1D** and **2R**.

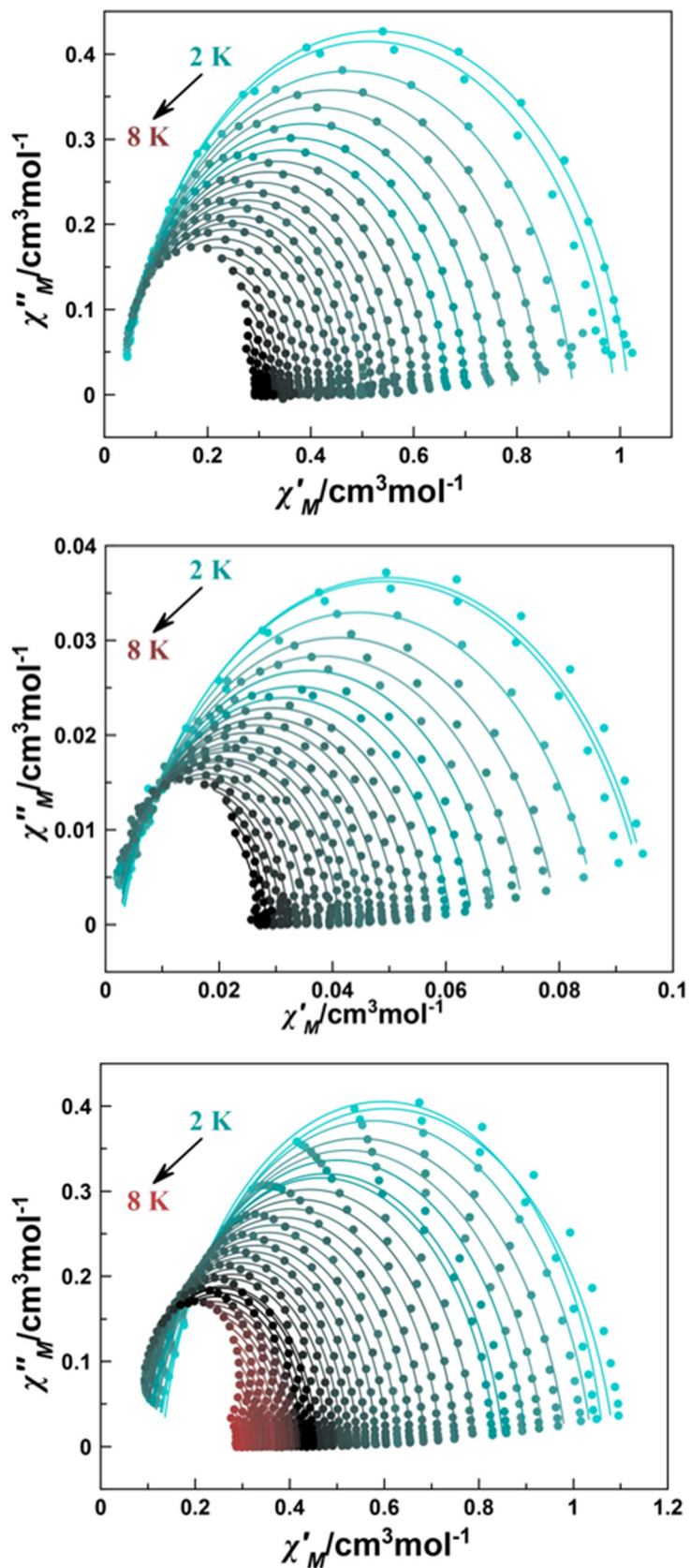


Fig. S10. Argand plots for complexes **1**, **1D** and **2R**. Solid lines show the best fit of the experimental data.

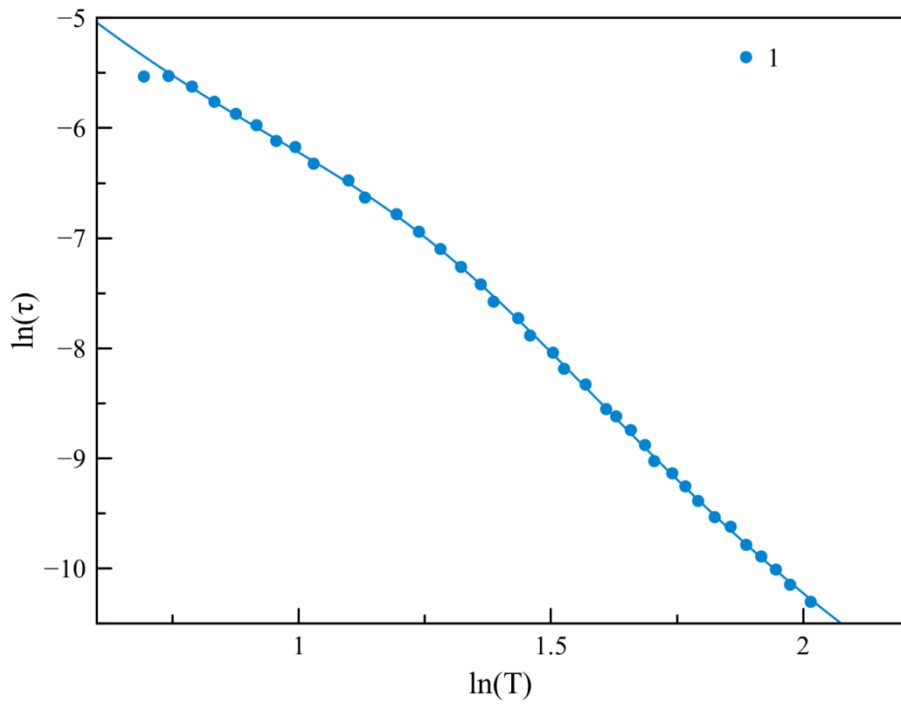


Fig. S11. Temperature dependence of the relaxation time of **1** plotted in log-log scale. The two different slopes at low and high temperature hints at dominant direct and Raman processes in the two temperature regions.

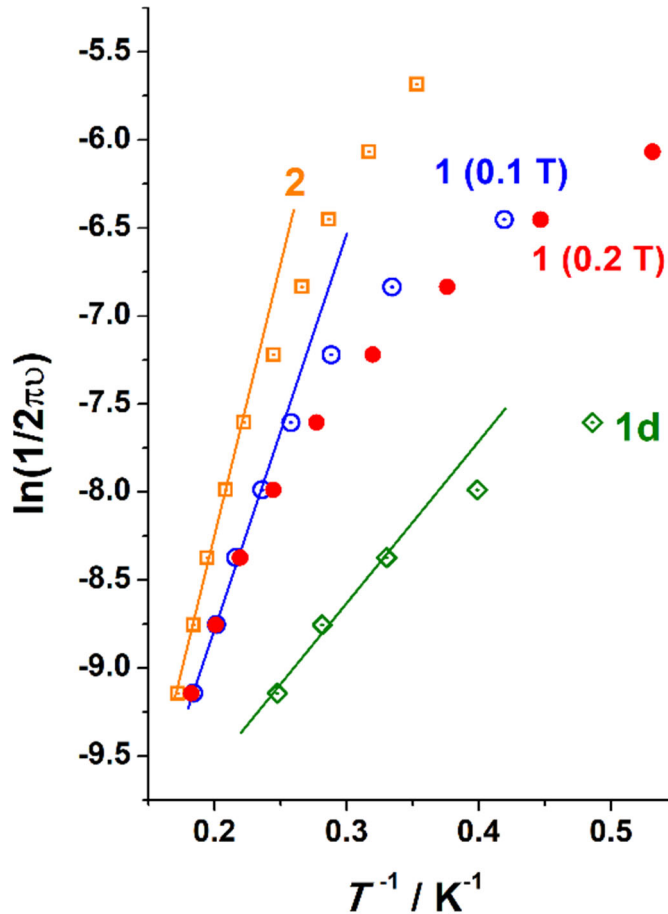


Fig. S12. Plot of $\ln(1/2\pi v)$ vs. T^{-1} from the $\chi_M''(T)$ data for complexes **1**, **1D** and **2R**. The data are limited to the HF region for which the maxima of χ_M'' can be observed.

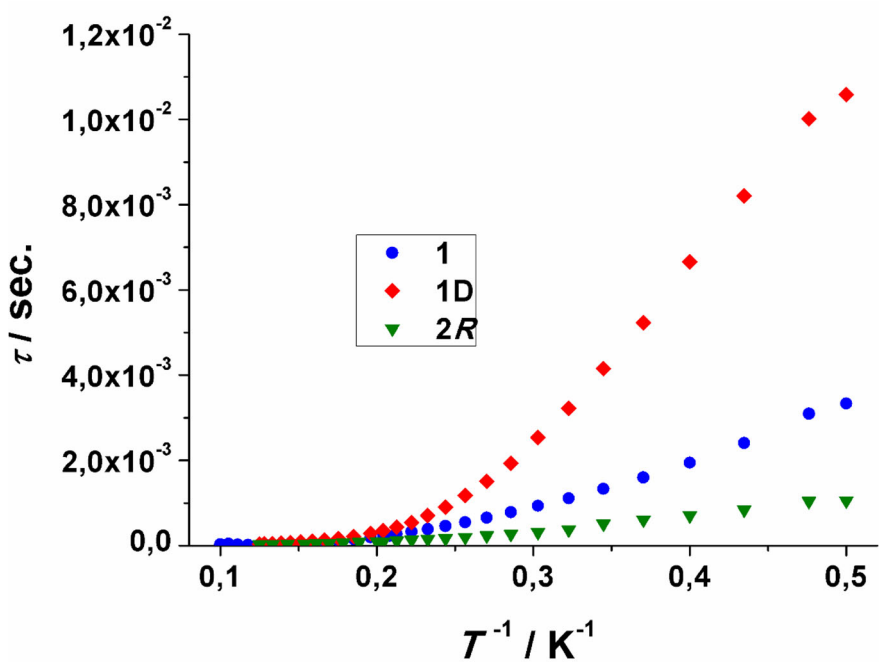


Fig. S13. Plot of τ vs. inverse of temperature showing the lowtemperature increase of t for the diluted complex **1D**.